Materials Physics and Mechanics. 2022;49(1): 160-172
Conference materials
http://dx.doi.org/10.18149/MPM.4912022_12

Rate-independent selection of slip patterns on grain and subgrain scales: state of the art

A.A. Zisman, N.Yu. Ermakova✉

Peter the Great St. Petersburg Polytechnic University, 29 Polytekhnicheskaya, St. Petersburg 195251, Russia

✉ ermakova@phmf.spbstu.ru

Abstract. To simulate the fragmentation of grains in cold deformed polycrystals, the underlying heterogeneity of crystal slip patterns should be quantified. Although it is understood that such patterns split owing to both the grain interaction and tendency to weaken the local strain hardening, properly justified numerical models for the considered effect are still wanted. This paper briefly surveys relevant extensions of rate-independent Taylor's theory and currently popular rate-sensitive formulations coupled with finite element modeling. Then, to exclude the limitations of such efforts, a novel rate-independent model is formulated that accommodates *macroscopic* deformation by the interfacial skeleton while suggesting specific slip patterns to keep the *local* strain compatibility across any grain boundary facet. Based on this approach, the fragmentation onset at grain junctions is predicted, and refinements of the model which should extend it to grain interiors are discussed.
Keywords: crystal fragmentation, dislocation boundary, plasticity, slip pattern, strain rate

Acknowledgements*. No external funding was received for this study.*

Citation: Zisman AA, Ermakova NYu. Rate-independent selection of slip patterns on grain and subgrain scales: state of the art. *Materials Physics and Mechanics*. 2022;49(1): 160-172. DOI: 10.18149/MPM.4912022_12.

1. Introduction

As shown by Rybin [1], the fragmentation of constitutive crystals into structural units separated by high-angle boundaries is a general regularity in polycrystals cold deformed to high strain degrees. Eventually detected on various metals [2-5], this effect attracts great attention because resulting ultrafine-grained structures provide extraordinary mechanical properties [4]. It is worth noting that piecewise uniform models extending the original Taylor's theory [6] still provide satisfactory predictions of the *overall* polycrystal texture even though they neglect the influence of the *local* orientation splitting [7]. Evidently, similar models average out related errors present on the grain scale; however, this simplification becomes irrelevant when the local grain fragmentation as such is considered.

It has been understood that the slip pattern and hence lattice orientation in deformed grains can split for two main reasons. First, this is the grain interaction effect indicated by TEM data [1] on triple grain junctions where deformation-induced dislocation boundaries nucleate and often branch toward grain boundaries. Similar behavior is also observed in the deformation of macroscopic tri-crystals [8]. A simplified 2D model [9] ascribes such events to the interaction of a primary slip system with various boundary facets that activates specific

secondary systems. Another reason for the considered splitting is that simultaneous activity of many slip systems in the same local domain would significantly increase the strain hardening and, accordingly, the plastic work. Meanwhile, unlike the uniform flow by five slip systems of any crystal [6], it is possible to accommodate the given strain rate by a set of simpler slip patterns operating in its fragments [2,10]. Such a concept is supported by the prevailing dependence of slip patterns in constitutive grains on their own orientations [11], as well as by heterogeneity of orientation and plastic shearing in deformed single crystals [12,13] free of the grain interaction. A tendency to weaken the local hardening is also manifested by the single slip in shear microbands [14] and plastic accommodation of martensite laths splitting into partial simple shears of their constituents [15,16].

The present paper briefly surveys the potentiality of various models for crystal plasticity from the standpoint of fragmentation. A crucial issue, in this case, is that slip patterns of adjacent crystal domains determining their emerging disorientation should be selected *uniquely*. Unambiguity of slip patterns on the grain scale is conventionally ensured by the rate-sensitive plasticity [17] admitting in any crystal activity of all its slip systems. However, let alone computational difficulties due to the weak rate sensitivity in cold deformation, such an approach does not comply with actual patterns of neighboring fragments, each involving only a few slip systems. To select the latter, a rate-independent model is formulated in terms of the deformed interfacial skeleton that keeps local strain compatibility across grain boundaries. It properly predicts the crystal fragmentation onset at triple grain junctions, and further refinements are discussed which should extend the model to the orientation splitting into grain interiors.

2. Taylor-Bishop-Hill theory

Current rate-independent models of plastically deformed polycrystals are based on the classical formulation by Taylor [6] while refining the latter in a way to allow for the grain interaction and to select crystal slip patterns. Although such models ignore the fragmentation effect, it is advisable to recollect some of their terms and relationships applicable to local in-grain domains. According to [6], the arbitrary plastic strain rate $\boldsymbol{D}_g$ of any grain is accommodated by five slip systems:

$$\boldsymbol{D}_g = \sum_{k=1}^{5} \dot{\gamma}_k (\boldsymbol{b}_k \otimes \boldsymbol{n}_k + \boldsymbol{n}_k \otimes \boldsymbol{b}_k)/2, \tag{1}$$

where $\dot{\gamma}_k$ are the related shear rates, $\boldsymbol{b}_k$ and $\boldsymbol{n}_k$ are the shear directions and unit normal vectors to slip planes, respectively; $\otimes$ means the tensor product. The corresponding tensor of plastic rotation rate with respect to the invariant crystal lattice is

$$\boldsymbol{W}_g = \sum_{k=1}^{5} \dot{\gamma}_k (\boldsymbol{n}_k \otimes \boldsymbol{b}_k - \boldsymbol{b}_k \otimes \boldsymbol{n}_k)/2. \tag{2}$$

Thus, if the total material spin $\boldsymbol{W}_g^{(T)}$ of the grain is given, the lattice rotation rate is expressed by

$$\boldsymbol{W}_g^{(L)} = \boldsymbol{W}_g^{(T)} - \boldsymbol{W}_g. \tag{3}$$

To treat the grain interaction in the simplest way, it has been presumed that

$$\text{(a) } \boldsymbol{D}_g = \boldsymbol{D}, \text{ (b) } \boldsymbol{W}_g^{(T)} = 0, \tag{4}$$

where $\boldsymbol{D}$ is the deviator part of macroscopic strain rate; however, these presumptions can be refined while saving general Eqs. (1) to (3). A challenging problem in the considered approach is that five active slip systems are selected from a greater number of candidates as, for instance, twelve in FCC crystals. Accordingly, an enormous multiplicity of C_{12}^5 selection variants should be checked. Moreover, although only combinations with the least amount of shear rates

$$\sum_{k=1}^{5} |\dot{\gamma}_k| = min \quad (5)$$

is admitted among them, the result remains *non-unique* and necessitates a random choice.

Corresponding to a certain shear resistance in all slip systems, Eq. (5) suggests the least plastic work on deformed grains and, as shown by Bishop and Hill [18], enables the model refinement in terms of the crystal yield surface. Facets of the latter correspond to the critical magnitude (CRSS) *s* of the resolved shear stresses (RSS)

$$\tau_i = \sigma_g : (\boldsymbol{n}_i \otimes \boldsymbol{b}_i) \quad (6)$$

in potential slip systems, where σ_g is the crystal stress tensor, and colon means the double scalar product. Thus, in the case of FCC lattice i=1, 2, …, 12 should be considered with Eq. (6). In this case, arbitrary $\boldsymbol{D}_g$ involves five slip systems from six or eight ones forming an apex of the crystal yield surface depending on the crystal orientation. As compared to Taylor's model, this diminishes the above-mentioned multiplicity to $C_6^5 = 6$ or $C_8^5 = 56$, respectively, although the previous non-uniqueness of the admitted selections is retained.

A principal origin of the considered ambiguity in the Tailor-Bishop-Hill (TBH) theory is Eq. (4a) which roughly extends an essentially *local* strain compatibility condition [19] to the interaction of whole finite crystals. The inaccuracy of this simplification is also evident in terms of the stress balance requirement. Indeed, contrary to the latter, any grain stress derived at a given $\boldsymbol{D}_g$ from the crystal orientation does not depend on stresses in neighboring grains. A natural way to improve the model in accordance with experimental data on cold deformed polycrystals is to allow for in-grain heterogeneity of plastic shearing. However, as considered in the next section, some approaches still provide a unique slip pattern while keeping uniformity of the crystal strain rate.

3. Unique selection of uniform slip pattern

To save the uniqueness of crystal slip patterns, different ways are used. The most popular one admits simultaneous activity of *all* potential slip systems depending on related RSS and thus avoids the selection multiplicity. Another approach refines constraint (5) excluding inactive slip systems in rate-independent models. We will consider below specific advantages and drawbacks of such expedients in application to crystal orientation splitting. A common complication of them is the cumbersome treatment of hardening in all (*k=1, 2, …, N*) slip systems. The general expression for time derivatives of related CRSS [20] is

$$\dot{s_k} = \sum_{n=1}^{N} h_{kn} |\dot{\gamma}_n|, \quad (7)$$

where $n = k$ and $n \neq k$ are due to the self-hardening and latent hardening, respectively. Let alone a great number $N^2$of h_{kn}, none of these coefficients is determined independently; instead, the whole set of them is fitted to the *macroscopic* stress-strain diagram that is hardly relevant to specific slip patterns of local in-grain fragments.

Rate-sensitive models. Following [17], the shear rate in whatever slip system number *k* is expressed by

$$\dot{\gamma}_k = \dot{\gamma}_o |\tau_k / s_k|^{1/m} sign(\tau_k), \quad (8)$$

where τ_k is its RSS, while *m* and $\dot{\gamma}_o$ are the rate sensitivity exponent and the reference strain rate, respectively. Suggesting activity of all slip systems in a stressed crystal, this expression provides its unique slip pattern. Moreover, since non-diagonal components (latent hardening) in matrix h_{kn} are generally higher [21], they weaken essentially formal contributions of systems with low RSS to the crystal strain and reorientation. Combined with the finite element method (FEM), this approach enables the modeling of heterogeneous plastic shearing in individual grains [13,22-24] while properly allowing for their interaction. At the same time, there are significant limitations as follows.

Eq. (8) is hard to apply in the case of cold deformation when *m* approaches zero [21]; this complicates the modeling on both the grain and in-grain scales. Computational expenses

become enormous when the latter is treated in 3D by the crystal plasticity FEM. Indeed, an actual polyhedral grain has about 20 facets separating it from its next neighbors which should be allowed for to simulate the grain interaction. Furthermore, since typical fragments have submicron to micron dimensions [1-5], respective models should subdivide each grain or a more representative cluster into at least 10^5 finite elements. Hence, to utilize the potentiality of the considered approach, it would be highly desirable to decompose the modeling into *separate* constitutive crystals with properly predetermined boundary conditions.

Rate-independent selection. According to Anand [21], the unique slip pattern of a single crystal subject to a given strain rate can be derived from the consistency condition

$$\dot{s_k} = |\dot{\tau_k}| \tag{9}$$

between time derivatives of CRSS, which change during the strain hardening, and those of respective RSS magnitudes, which follow both the variation of deforming stress and gradual reorientation of the crystal. Among virtual selections satisfying Eq. (9), the unique pattern found by a special algebraic approach suggests the least quadric norm of shear rates:

$$\sum_{k=1}^{N} \dot{\gamma_k}^2 = min, \tag{10}$$

where the contributions of inactive slip systems are zero. Accordingly, the substitution of the latter norm for Eq. (5) could reduce the ambiguity of slip patterns in Taylor's theory. Although the physical sense of Eq. (10) wants clarification, the considered rate-independent model, as well as its modifications [25,26] can be used to avoid the slip pattern uncertainty in the piecewise-uniform approach to plastically deformed polycrystals. However, they still do not allow for crystal orientation splitting.

4. Local strain compatibility across interfaces

To refine the treatment of strain compatibility between grains, this constraint should be adjusted to each specific facet of a grain boundary. When applied to a planar interface with normal vector $\boldsymbol{N}$, the general compatibility equation [19] comes to

$$\boldsymbol{H}_N = \boldsymbol{N} \times (\boldsymbol{D}^+ - \boldsymbol{D}^-) \times \boldsymbol{N} = \boldsymbol{0}, \tag{11}$$

where the strain rates $\boldsymbol{D}^+$ and $\boldsymbol{D}^-$ are due to the adjacent domains indicated by $\boldsymbol{N}$ and (-$\boldsymbol{N}$), respectively, and × means the vector product. According to Kröner [27], any plastic incompatibility $\boldsymbol{H}_N \neq \boldsymbol{0}$ is accommodated by an elastic strain field; in other words, the related boundary area becomes a two-dimensional source of internal stresses. Excluding the latter, Eq. (11) suggests equal planar projections of $\boldsymbol{D}^+$ and $\boldsymbol{D}^-$ i.e. similar strain rates of the boundary sides. This requirement applies to whichever *inelastic* strains. For instance [28], a collective effect of the lattice transformation and accommodative plastic shears in emerging martensite crystals is presumed to keep "invariant plane strains" for their habits. It is worth noting that a planar symmetric strain has only three independent components so that several components of tensor $\boldsymbol{D}^+ - \boldsymbol{D}^-$ do not affect the interfacial strain compatibility. Accordingly, the "relaxed constraint" of heavily flattened grains [29] enables their simplified slip patterns.

Along with the local influence of the grain interaction tractable by Eq. (11), another special constraint should be employed to accommodate the given *macroscopic* deformation of a polycrystal. As considered in the next section, simultaneous allowance for the two issues is provided by cluster models. Besides, to avoid their limitations and facilitate the modeling, a novel approach to the same problem will be introduced in Section 7.

5. Cluster models

Complying with Eq. (11), the simplest cluster model called LAMEL [30] accommodates macroscopic strain rate by any couple of plate-like grains separated by a boundary parallel to a rolling plane. To simulate the overall polycrystal texture at high degrees of thickness reduction, this rate-independent model treats one by one various virtual bicrystals whose orientation statistics correspond to the given initial texture. Unlike ten active slip systems in

each couple according to Taylor's model, the partitioning of the imposed strain rate reduces their number to eight. Moreover, opposite shear rates of the two halves along the boundary, admitted by the interfacial compatibility, are selected to minimize the number of shear rates in the considered systems. The model has been eventually extended to admit various orientations of the planar interfaces [31] which gradually change their fractions following the grain shape. A more general approach of this sort [32] can involve the cluster whatever presumed number of constitutive grains.

As previously mentioned, statistical characteristics of the overall texture may implicitly allow for the in-grain orientation heterogeneity. Thus, a question appears of whether slip patterns splitting on the in-grain scale can be directly revealed in terms of the cluster concept. Such an effort [33] motivating the extension [31] of LAMEL model has been applied to thin bicrystals at the grain boundary facets, while a remaining part of the grain has been treated in terms of Taylor's model. As expected, the local slip patterns and resulting lattice orientations within the same crystal sharply split near triple junction lines. However, this interesting work still does not find any development because of some challenging issues. First, there is no rigorous criterion to select the thickness of the plate-like fragments. Second, it is not at all evident that their thin couples follow macroscopic strain rate. The latter issue gains in significance since the related disorientation strongly depends on the local distribution of plastic shearing. Finally, yet importantly, it is unclear how to extend this model to the eventual fragmentation of grain interiors.

6. Successive selection of active slip systems

It has been understood long ago [9,34] that the multi-slip gradually develops in disoriented constitutive crystals owing to their mutual plastic accommodation. There are two important aspects of this concept concerning crystal fragmentation. First, the local interaction of grains across their boundaries suggests a particular slip pattern at any interfacial facet; as considered in Section 7, such patterns trigger the orientation splitting near grain junctions. Second, each next slip system of a crystal is activated because of the strain mismatch and related reactive stress accumulated during the activity of the previous (incomplete) selection. We will make use of the successive activation events to quicken the selection of the final pattern. The algorithm does not follow the process in time; however, the whole sequence of its steps is explicitly reflected. As shown in the next section, simple combinations ($N<5$) of slip systems sought at the respective steps are relevant to local fragments near grain boundaries. Meanwhile, to better understand the formal grounds of this approach, it is reasonable to consider first a uniformly deformed crystal. For a case study, under consideration is the macroscopic strain rate tensor

$$\boldsymbol{D} = D\begin{pmatrix} 1 & 0 & 0 \\ 0 & -1 & 0 \\ 0 & 0 & 0 \end{pmatrix} \tag{12}$$

roughly corresponding to the rolling. Axes of related Cartesian system XYZ are parallel to the rolling, normal, and transversal directions, respectively. Table 1 numbers treated slip systems $\{111\}\langle 110\rangle$ of the FCC lattice.

Any local orientation is expressed by the rotation matrix $\boldsymbol{R}$ matching XYZ to the considered crystal domain; this matrix is derived as elsewhere from local crystallographic indices of the rolling plane (ND) and direction [RD]. Accordingly, normalized Burgers vectors $\boldsymbol{b}_i$ and normal vectors $\boldsymbol{n}_i$ to slip planes ($i = 1, 2, \ldots, 12$) are determined in terms of their reference counterparts corresponding to Table 1:

$$\boldsymbol{b}_i = \boldsymbol{R}\boldsymbol{b}_i^{(o)}, \boldsymbol{n}_i = \boldsymbol{R}\boldsymbol{n}_i^{(o)}. \tag{13}$$

The *active* slip systems are successively marked by subscripts $k = 1 \div 5$ which may differ from related numbers the table. Each of them is specified by the symmetric strain direction tensor

$$\boldsymbol{d}_k = (\boldsymbol{b}_k \otimes \boldsymbol{n}_k + \boldsymbol{n}_k \otimes \boldsymbol{b}_k)/2, \quad (14)$$

and the selection procedure makes use of Taylor's approximation (Eq. (4a) for the strain compatibility.

Table 1. Employed numeration of slip systems in FCC lattice

Number	1	2	3	4	5	6	7	8	9	10	11	12
Slip plane	(111)	(111)	(111)	$(\bar{1}11)$	$(\bar{1}11)$	$(\bar{1}11)$	$(1\bar{1}1)$	$(1\bar{1}1)$	$(1\bar{1}1)$	$(11\bar{1})$	$(11\bar{1})$	$(11\bar{1})$
Slip direction	$[01\bar{1}]$	$[10\bar{1}]$	$[1\bar{1}0]$	$[101]$	$[110]$	$[01\bar{1}]$	$[011]$	$[110]$	$[10\bar{1}]$	$[011]$	$[101]$	$[1\bar{1}0]$

The first active system is selected to provide the maximum contribution to $\boldsymbol{D}$ i.e.

$$|\boldsymbol{d}_1 : \boldsymbol{D}| = max\{|\boldsymbol{d}^{(i)} : \boldsymbol{D}|\}, \quad (15)$$

where superscript (i) the strain direction tensors of trial slip systems according to Table 1. In the case of several admitted variants, a random choice should be made, and the same rule remains valid at other steps ($k > 1$). The selection of slip patterns with the least deviation from $\boldsymbol{D}$ somewhat complicates the second to fourth steps. In algebraic terms, it suggests the maximum orthogonal projection of $\boldsymbol{D}$ on the linear space generated by the current set $\{\boldsymbol{d}_1, \dots, \boldsymbol{d}_k\}$ of direction tensors. To satisfy this condition, the procedure is repeated as follows at $k = 2, 3, 4$ with the same $\boldsymbol{p}_1 = \boldsymbol{d}_1$. Orthogonal to $\boldsymbol{d}_1, \dots, \boldsymbol{d}_{k-1}$, the virtual basic tensors

$$\boldsymbol{p}_k^* = \boldsymbol{d}_k^* - \boldsymbol{p}_1(\boldsymbol{d}_k^* : \boldsymbol{p}_1)/(\boldsymbol{p}_1 : \boldsymbol{p}_1) - \dots - \boldsymbol{p}_{k-1}(\boldsymbol{d}_k^* : \boldsymbol{p}_{k-1})/(\boldsymbol{p}_{k-1} : \boldsymbol{p}_{k-1}) \quad (16)$$

are determined first for all trial $\boldsymbol{d}_k^*$; next, acceptable $\boldsymbol{d}_k$, $\boldsymbol{p}_k$ and respective $\boldsymbol{D}_k$ are found to get

$$\boldsymbol{D}_k : \boldsymbol{D}_k = max\{\boldsymbol{D}_k^* : \boldsymbol{D}_k^*\} \quad (17)$$

where

$$\boldsymbol{D}_k^* = \boldsymbol{p}_1(\boldsymbol{D} : \boldsymbol{p}_1)/(\boldsymbol{p}_1 : \boldsymbol{p}_1) + \dots + \boldsymbol{p}_{k-1}(\boldsymbol{D} : \boldsymbol{p}_{k-1})/(\boldsymbol{p}_{k-1} : \boldsymbol{p}_{k-1}) + \boldsymbol{p}_k^*(\boldsymbol{D} : \boldsymbol{p}_k^*)/(\boldsymbol{p}_k^* : \boldsymbol{p}_k^*). \quad (18)$$

Since $\boldsymbol{d}_j : \boldsymbol{p}_m = 0$ at any $j < m$, the partial shear rates $\dot{\gamma}_m$ $(m = 1, 2, \dots, k)$ are simply expressed by

$$\dot{\gamma}_m = (\boldsymbol{D}_m : \boldsymbol{p}_m)/(\boldsymbol{d}_m : \boldsymbol{p}_m). \quad (19)$$

To further weaken ambiguity at intermediate steps ($2 \le k \le 4$), one more constraint is applied:

$$\Gamma_k = |\dot{\gamma}_1| + \dots + |\dot{\gamma}_k| = min. \quad (20)$$

To exclude at $k \ge 3$ the slip systems geometrically dependent on previously selected ones, each

$$\boldsymbol{d}_k^* = \boldsymbol{p}_1(\boldsymbol{p}_1 : \boldsymbol{d}_k^*)/(\boldsymbol{p}_1 : \boldsymbol{p}_1) + \dots + \boldsymbol{p}_{k-1}(\boldsymbol{p}_{k-1} : \boldsymbol{d}_k^*)/(\boldsymbol{p}_{k-1} : \boldsymbol{p}_{k-1}) \quad (21)$$

is rejected.

At the last step, $\boldsymbol{D}$ can be accommodated by whatever available set of five slip systems. Among such patterns, only those with the least shear amount are admitted according to Eq. (5). Figure 1 shows the sequential selections at orientations $(\mathrm{ND})[\mathrm{RD}] = (23\bar{1})[115]$ and

$(\mathrm{ND})[\mathrm{RD}] = (123)\left[36\bar{5}\right]$. Note that some intermediate slip systems suggested by the least incompatibility criterion have been excluded because of additional requirements (20).

According to Eq. (6), the rate-independent approach [6,18] suggests RSS in active slip systems $m = 1 \div 5$ is equal to certain CRSS-s. Since the RSS depend only on the deviator $\sigma'$of the grain stress σ_g, the former can be derived from

$$\sigma' : \boldsymbol{d}_m = s \qquad (22)$$

that comes to five simultaneous equations in five unknowns because $\sigma'_{33} = -\sigma'_{11} = \sigma'_{22}$. As soon as σ' is found, RSS in all remaining slip systems ($i \neq m$) is determined by substitution of $\boldsymbol{d}^{(i)}$ for $\boldsymbol{d}_m$ and the sought τ_i for s in the same Eq. (22). In what follows, this enables the comparison of our algorithm with the Taylor-Bishop-Hill (TBH) theory.

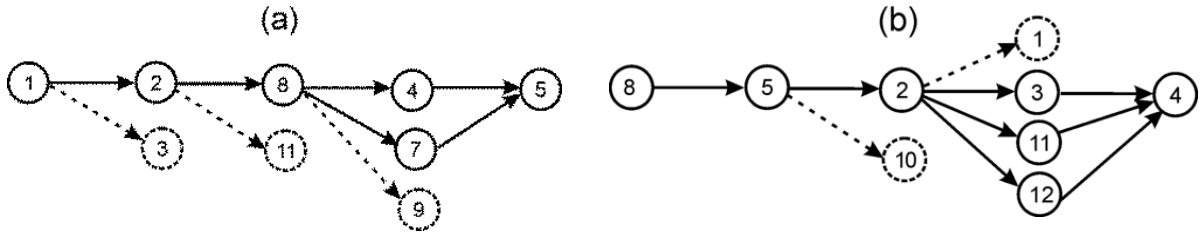

Fig. 1. Selection of active slip systems at crystal orientations (a) $(\mathrm{ND})[\mathrm{RD}] = (23\bar{1})[115]$ and (b) $(\mathrm{ND})[\mathrm{RD}] = (123)\left[36\bar{5}\right]$. Dash arrows indicate systems rejected because of excessive amount of shear rates at related steps

Table 2 represents numerical simulation results at orientation $(\mathrm{ND})[\mathrm{RD}] = (23\bar{1})[115]$; for brevity's sake, they are shown only for one of the two slip patterns (Fig. 1a) coinciding with Taylor's selections which have the least sum $\dot{\Gamma} = 2.829$ of shear rate magnitudes. In the second pattern slip system 7, previously *potentially* active ($|\tau|/s = 1$ but $\gamma = 0$), substitutes active system 4. Although in this case $\dot{\Gamma}$ remains the same, the underlying set of partial shear rates changes. According to Table 2, $|\tau|$ reaches s in *six* slip systems whereas, as considered below, another crystal orientation suggests *eight* ones. These findings comply with a specific property of FCC crystals according to the TBH theory where any apex of the yield surface [18] involves six or eight slip systems depending on the lattice orientations. Besides, as previously noted in [35], RSS in all *inactive* ($|\tau| < s$) slip systems of our crystals proved to vanish.

Table 2. RSS and magnitudes of related shear rates at orientation $(\mathrm{ND})[\mathrm{RD}] = (23\bar{1})[115]$

Slip system	Active*					Potential	Inactive					
	1	2	8	4	5	7	3	6	9	10	11	12
τ/s	-1	-1	1	1	1	1	0	0	0	0	0	0
$\lvert\dot{\gamma}\rvert/D$	0.872	1.134	0.674	0.086	0.062	0	0	0	0	0	0	0

*In order of selection

The simulation results shown in Table 3 are due to orientation $(\mathrm{ND})[\mathrm{RD}] = (123)\left[36\bar{5}\right]$ that suggests the yield surface apex formed by *eight* slip systems (active and potentially active) with $|\tau|/\tau_c = 1$. Unlike the previous $\mathrm{C}_6^5 = 6$, in this case, the TBH approach should check $\mathrm{C}_8^5 = 56$ sets of five slip systems. This is much more computationally expensive than our algorithm that compares steps 3 and 4 (Fig. 1b) with only $2 + 4 = 6$ potential variants of incomplete ($k < 5$) slip patterns. Thus, as the constitutive grains of the polycrystal generally have comparable fractions of both orientation types, the sequential selection enables much quicker simulations of the texture development. Although the algorithm finds almost all slip

patterns of Taylor's type, the above-mentioned complex combinatorics some of them can be missed since they do not provide the least strain rate incompatibility in selection steps 2 to 4. For instance, the least $\Gamma = 4.199$ given by each of the found selections (Fig. 1b) is also the case when slip system 3 in the considered set is substituted by system 9 although the latter is excluded by our algorithm for the above-mentioned reason. To assess the statistical significance of such cases, it is advisable to consider related polycrystal textures.

Table 3. RSS and magnitudes of related shear rates at orientation $(\mathrm{ND})[\mathrm{RD}] = (123)[36\bar{5}]$

Slip	Active*					Potential			Inactive			
system	8	5	2	3	4	9	11	12	1	6	7	10
τ/s	-1	-1	1	1	-1	-1	-1	-1	0	0	0	0
$\lvert\dot{\gamma}\rvert/D$	2.030	0.770	0.630	0.700	0.070	0	0	0	0	0	0	0

*In order of selection

Both the TBH model and the present method have been applied with strain increments of 0.01 to predict the texture of an FCC polycrystal subject to the thickness reduction of 50% at $\boldsymbol{D}$ expressed by Eq. (12). A random distribution of 5000 crystal orientations was generated for the initial state, and the only difference between two approaches was in a way to select active slip systems of constitutive grains. Table 4 lists the resulting fractions of texture components calculated within angular deviations of 15° from the indicated orientations. As expected, the rare slip systems admitted in the TBH model, but excluded by our algorithm, affect the predicted results rather weakly. We do not display respective pole figures because it would be hardly possible to distinguish between them. Note that the likeness of these textures confirms the statistical similarity of related slip patterns even though at high strains each of the two approaches loses accuracy because the grain flattening is neglected. Limited to *uniform* crystals, the grain shape effect is tractable by extensions [29,30] of the original TBH theory; however, they are also unable to predict the fragmentation of plastically deformed crystals into disoriented parts.

Table 4. Predicted fractions of rolling texture components (per cent) in a FCC polycrystal at 50 % thickness reduction

Texture component	{110} ⟨001⟩	{110} ⟨112⟩	{211} ⟨111⟩	{123} ⟨634⟩	{100} ⟨001⟩
Present model	4.3	9.5	20.4	34.5	1.6
TBH model	4.0	9.4	20.0	33.8	1.6

To sum up this section, the considered approach quickens the selection of active slip systems while its essentially *geometrical* formulation avoids the poorly justified treatment of CRSS variations in strain hardening as well as specific limitations of rate-sensitive models. Although Taylor's problem of slip pattern ambiguity still has been retained, on the local scale at grain boundaries it can be resolved as demonstrated in what follows.

7. Model of deformed interfacial skeleton

While maintaining the *local* strain compatibility across grain boundaries considered in Section 4, a polycrystal should accommodate *macroscopic* deformation. To satisfy these two requirements at once, we will make use of a simple approximation. It presumes that the interfacial skeleton follows a macroscopic strain rate whichever in-grain heterogeneities and projection of $\boldsymbol{D}$ onto any boundary facet is accommodated at both its sides to keep the interfacial compatibility. Since a symmetric planar strain has three independent components,

three slip systems in each of the two differently oriented crystalline domains will be sufficient to satisfy the latter condition.

Specific details of the proposed scheme are available elsewhere [36]; briefly, the previous tensor terms and related procedures minimizing the strain rate incompatibility are projected on planar boundary facets. According to Fig. 2, a trial simulation has been implemented at the perfect (120°) junction of three grain boundaries parallel to axis Z. Normal vectors to the considered facets are $\boldsymbol{N}_I = [-1/2, \sqrt{3}/2, 0]$ and $\boldsymbol{N}_{II} = [1/2, \sqrt{3}/2, 0]$ while the crystal orientation is specified by $(\mathrm{ND})[\mathrm{RD}] = (123)[36\bar{5}]$. Respective planar projections of the macroscopic strain rate $\boldsymbol{D}$ are denoted in Fig. 2 by $\boldsymbol{S}_I$ and $\boldsymbol{S}_{II}$, and other terms correspond to local strain rates and underlying slip systems.

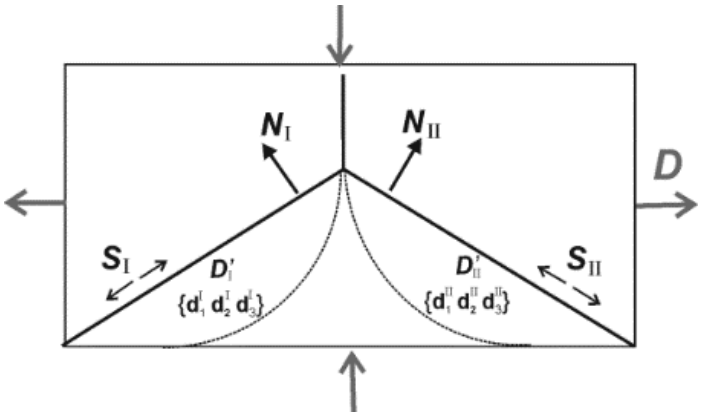

Fig. 2. Scheme to derive local slip patterns near grain boundary facets

Table 5 lists simulation results at $\boldsymbol{D}$ according to Eq. (12) for two adjacent domains of the same grain situated near the considered junction. $\boldsymbol{D}'$ and $\boldsymbol{w}'$ in this table are the local tensors of plastic strain rate and the vector of the plastic rotation rate, respectively; $\dot{\gamma}$ represents the shear rates in operating slip systems. It should be underlined that each of the predicted slip patterns proved to be *unique* although the number C_8^3 of potential variants was equal to C_8^5 in the case of Taylor's selection. Such a meaningful distinction is mostly due to one more constraint (orientation of a boundary plane) at the same strain rate and crystal orientation; besides, unlike five of Taylor's slip systems, the considered three suggest a lesser multiplicity of virtual selections.

Table 5. Simulation results for two neighboring domains of same grain (Fig. 2)

Domain	I			II		
Slip systems	1	2	9	5	9	11
$\dot{\gamma}/D$	1.019	0.043	0.156	−0.735	−0.123	−0.733
$\boldsymbol{D}'/D$	$\begin{pmatrix} 0.211 & 0.455 & 0.099 \\ 0.455 & -0.211 & -0.171 \\ 0.099 & -0.171 & 0 \end{pmatrix}$			$\begin{pmatrix} 0.243 & -0.437 & 0.014 \\ -0.437 & -0.243 & 0.024 \\ 0.014 & 0.024 & 0 \end{pmatrix}$		
$\boldsymbol{w}'/D$	[0.072	−0.235	0.481]	[0.192	−0.387	0.066]

To make use of $\boldsymbol{D}'$ and $\boldsymbol{w}'$ found in the considered fragments, respective increments of plastic strain and rotation during a small thickness reduction Δ expressed with Eq. (12) are kept in mind:

$$\boldsymbol{\varepsilon} = \boldsymbol{D}'\Delta/D, \boldsymbol{\omega} = \boldsymbol{w}'\Delta/D. \quad (23)$$

Given a plane (unit normal vector $\boldsymbol{N}'$) for a virtual dislocation boundary separating these two fragments, the corresponding increment of their disorientation vector is evaluated according to [37]:

$$\boldsymbol{\theta}' = \boldsymbol{N}' \times (\boldsymbol{\varepsilon}_{II} - \boldsymbol{\varepsilon}_I) \cdot \boldsymbol{N}' + \boldsymbol{\omega}_I - \boldsymbol{\omega}_{II} \quad (24)$$

where the dot indicates a scalar product. However, although a fresh boundary emerging near the grain junction may be revealed by means of electron microscopy; further refinements of the model are required to *predic*t $\boldsymbol{N}'$absent in Fig. 2.

To roughly assess the likelihood of the found patterns (Table 5), the contribution of $\boldsymbol{\omega}_I$ and $\boldsymbol{\omega}_{II}$ to $\boldsymbol{\theta}'$ has been calculated at $\Delta = 0.1$:

$$\boldsymbol{\theta}'_\omega = 2.6°[-0.262 \quad 0.332 \quad 0.906], \quad (25)$$

and its magnitude (angle) seems to be realistic for a dislocation boundary nucleating at the junction line. Next, a *virtual* boundary plane YZ (bisector of the lower grain in Fig. 2) has been presumed to assess the effect of plastic strain discontinuity. According to Eq. (24), it induces

$$\boldsymbol{\theta}'_\varepsilon = 5.1°[0 \quad 0.095 \quad -0.996] \quad (26)$$

whereas resulting disorientation vector

$$\boldsymbol{\theta}' = \boldsymbol{\theta}'_\varepsilon + \boldsymbol{\theta}'_\omega = 3.1°[-0.220 \quad 0.434 \quad -0.874] \quad (27)$$

still has a plausible magnitude.

To sum up, this work based on the least strain incompatibility criterion, a quick algorithm is formulated to select one by one active slip systems of a deformed crystal. When tested on virtually uniform slip patterns of whole grains, this approach generally finds Taylor's slip patterns with the least shear amount. When applied to the local domains at grain boundaries, it quantifies the related in-grain heterogeneity of plastic shearing and thus enables simulations of the crystal fragmentation onset.

8. Concluding remarks

The main limitation of the considered approach focused on local slip patterns near grain boundaries is that it ignores the orientation splitting into grain interiors. In principle, the problem is tractable by the crystal plasticity FEM; however, representative clusters of subdivided grains conventionally treated by this method suggest an excessive computational cost. Meanwhile, the interfacial skeleton concept seems to admit the model decomposition into separate constitutive crystals. Although this challenging issue is beyond the scope of the present paper, some expedients deserve discussion as follows.

Given CRSS *s*, the order tensor $\boldsymbol{C}^{-1}$of elastic compliance and grain boundary plane $\boldsymbol{N}$ prescribing a local slip pattern, the method of Lagrange multipliers enables the determination of related stress $\boldsymbol{\sigma}_N$. To this end, the density of elastic energy

$$e = \boldsymbol{\sigma}_N : \boldsymbol{C}^{-1} : \boldsymbol{\sigma}_N / 2 \quad (28)$$

should be minimized at constraint equalities ($k = 1, 2, 3$)

$$\boldsymbol{\sigma}_N : \boldsymbol{d}_k - s = 0 \quad (29)$$

due to the active slip systems Then, to mimic the interaction of grain with surroundings, specific forces (stress vectors)

$$\boldsymbol{f}_N = \boldsymbol{\sigma}_N \cdot \boldsymbol{N} \quad (30)$$

applied to its facets will provide boundary conditions enabling its *individual* modeling by the crystal plasticity FEM.

A remark should be made that these equations as well as the whole formulation are due to a *fixed* state of the deformed polycrystal whereas the fragmentation process develops over a rather wide strain range. Accordingly, the latter should be subdivided into small increments approximately keeping certain interfacial configurations, local crystal orientations, and respective slip patterns. It is easy to repeatedly upgrade grain shapes that follow macroscopic deformation; as to the lattice rotations accumulated in each increment at the fixed boundary

facets, they can be quantified as in the case of constrained martensite crystals described elsewhere [16].

References

1. Rybin VV. *Large Plastic Strains and Fracture of Metals*. Moscow: Metallurgy; 1986. (In Russian)
2. Bay B, Hansen N, Hughes DA, Kuhlmann-Wilsdorf D. Overview No. 96: evolution of f.c.c. deformation structures in polyslip. *Acta Metallurgica et Materialia*. 1992;40(2): 205-219.
3. Humphreys FJ, Bate PS. The microstructures of polycrystalline Al–0.1Mg after hot plane strain compression. *Acta Materialia*. 2007;55(16): 5630-5645.
4. Valiev RZ, Korznikov AV, Mulyukov RR. Structure and properties of ultrafine-grained materials produced by severe plastic deformation. *Materials Science and Engineering: A*. 1993;168(2): 141-148.
5. Chen SF, Li DY, Zhang SH, Han HN, Lee HW, Lee MG. Modelling continuous dynamic recrystallization of aluminum alloys based on the polycrystal plasticity approach. *International Journal of Plasticity*. 2020;131: 102710.
6. Taylor GI. Plastic strains in metals. *Journal of the Institute of Metals*. 1938;62: 307-324.
7. Seefeldt M, Van Houtte P. Grain subdivision and local texture evolution studied by means of a coupled substructure-texture evolution model. *Materials Science Forum*. 2002;408-412: 433-438.
8. Rey C, Mussot P, Vroux AM, Zaoui A. Effects of interfaces on the plastic behavior of metallic aggregates. *Journal de Physique Colloques*. 1985;46(C4): 645-650.
9. Berveiller M, Bouaquine H, Fakri N, Lipinski P. Texture transition, micro shear bands and heterogeneous plastic strain in FCC and BCC metals. *Textures and Microstructures*. 1988;8-9: 351-379.
10. Ananthan VS, Leffers T, Hansen N. Characteristics of second generation microbands in cold-rolled copper. *Scripta Metallurgica et Materialia*. 1991;25: 137-142.
11. Zaefferer S, Kuo JC, Zhao Z, Winning M, Raabe D. On the influence of the grain boundary misorientation on the plastic deformation of aluminium bicrystals. *Acta Materialia*. 2003;51: 4719-4735.
12. Wert JA, Liu Q, Hansen N. Dislocation boundary formation in a cold rolled cube-oriented Al single crystal. *Acta Materialia*.1997;45(6): 2565-2576.
13. Wei P, Zhou H, Liu H, Zhu C, Wang W, Deng G. Investigation of grain refinement mechanism of nickel single crystal during high pressure torsion by crystal plasticity modeling. *Materials*. 2019;12(3): 351.
14. Zisman A, Nesterova E, Rybin V, Teodosiu C. Interfacial misorientations and underlying slip activity of a shear microband in mild steel: TEM analysis and numerical simulation. *Scripta Materialia*. 2002;46: 729-733.
15. Ball J, James R. Fine phase mixtures as minimizer of energy. *Archive for Rational Mechanics and Analysis*. 1987;100: 13-52.
16. Zisman A. Predictive micromechanical model for plastic accommodation and crystallography of martensite embryo. *International Journal of Engineering Science*. 2020;150: 103245.
17. Asaro RJ, Needleman A. Texture development and strain hardening in rate dependent polycrystals. *Acta Metallurgica*. 1985;33: 923-953.
18. Bishop JFW, Hill R. A theory of the plastic distortion of a polycrystalline aggregate under combined stresses. *Philosophical Magazine*. 1951;42: 414-427.

19. Navier M, Saint-Venant B. *Résumé des Lecons Données à École des Ponts et Chaussées sur l'Application de la Mécanique à l'Etablissement des Constructions et des Machines*. Paris: Dunod; 1864.
20. Hill R. Generalized constitutive relations for incremental deformation of metal crystals by multislip. *Journal of the Mechanics and Physics of Solids*. 1966;14: 95-102.
21. Anand L, Kothari M. A computational procedure for rate-independent crystal plasticity. *Journal of the Mechanics and Physics of Solids*. 1996;44: 525-558.
22. Knezevic M, Drach B, Ardljan M, Beierlein IJ. Three dimensional predictions of grain scale plasticity and grain boundaries using crystal plasticity finite element models. *Computational Methods in Applied Mechanics and Engineering*. 2014;277: 239-259.
23. Roters F, Eisenlohr P, Hantcherli L, Tjahjanto DD, Bieler TR, Raabe D. Overview of constitutive laws, kinematics, homogenization and multiscale methods in crystal plasticity finite-element modeling: Theory, experiments, applications. *Acta Materialia*. 2010;58: 1152-1211.
24. Li S, Donohue BR, Kalidindi SR. A crystal plasticity finite element analysis of cross-grain deformation heterogeneity in equal channel angular extrusion and its implications for texture evolution. *Materials Science and Engineering: A*. 2008;480(1-2): 17-23.
25. Petryk H, Kursa M. Incremental work minimization algorithm for rate-independent plasticity of single crystals. *International Journal for Numerical Methods in Engineering*. 2015;104(3): 157-184.
26. Orthaber M, Antretter T, Gänser H-T. On the selection of active slip systems in rate independent crystal plasticity. *Key Engineering Materials*. 2013;554-557: 1147-1156.
27. Kröner E. *Kontinuumstheorie der Versetzungen und Eigenspanungen (Ergebnisse der Angewandten Mathematik, 5)*. Berlin: Springer; 1958.
28. Bullough R, Bilby BA. Continuous distribution of dislocations: Surface dislocations and crystallography of martensitic transformation. *Proceedings of the Royal Society of London*. 1956;B69: 1276-1286.
29. Kocks UF, Chandra H. Slip geometry in partially constrained deformation. *Acta Metallurgica*. 1982;30: 695-709.
30. Van Houtte P, Delannay L, Samaidar I. Quantitative prediction of cold rolling textures in low carbon steels by means of the LAMEL model. *Textures and Microstructures*, 1999;31: 109-149.
31. Van Houtte P, Li S, Seefeldt M, Delannay L, Samaidar I. Deformation texture prediction: From the Taylor model to the advanced Lamel model. *International Journal of Plasticity*. 2005;21: 589-624.
32. Raabe D. Simulation of rolling textures of bcc metals considering grain interactions and crystallographic slip on {110}, {112} and {123} planes. *Materials Science and Engineering: A*. 1995;197: 31-37.
33. Evers LP, Parks DM, Brekelmans WAM, Geers MGD. Crystal plasticity model with enhanced hardening by geometrically necessary dislocation accumulation. *Journal of the Mechanics and Physics of Solids*. 2002;50: 2403-2424.
34. Budiansky B, Wu TT. Theoretical prediction of plastic strains of polycrystals. In: Rosenberg RM. (ed.) *Proceedings of the 4th U.S. National Congress on Applied Mechanic*s. New York: ASME; 1962. p.1175-1185.
35. Clausen B, Leffers T, Lorentzen L, Pedersen OB, Van Houtte P. The resolved shear stress on the non-active slip systems in Taylor/Bishop-Hill models for FCC polycrystals. *Scripta Materialia*. 2000;42: 91-96.
36. Zisman A. Model for partitioning slip patterns at triple junctions of grains. *International Journal of Engineering Science*. 2017;116: 155-164.

37. Zisman AA, Rybin VV. Basic configurations of interfacial and junction defects induced in a polycrystal by deformation of grains. *Acta Materialia*. 1996;44(1): 403-407.

THE AUTHORS

Alexander A. Zisman
e-mail: azisman@spbstu.ru
ORCID: 0000-0002-9431-7097

Natalia Yu. Ermakova
e-mail: ermakova@phmf.spbstu.ru
ORCID: 0000-0002-1324-7112